Available online at www.sciencedirect.com
SCIENCE DIRECT®
Journal of Solid State Chemistry 170 (2003) 154–164
JOURNAL OF SOLID STATE CHEMISTRY
http://elsevier.com/locate/jssc

Tolerance factor rules for $Sr_{1-x-y}Ca_xBa_yMnO_3$ perovskites

B. Dabrowski,[a,*] O. Chmaissem,[a] J. Mais,[a] S. Kolesnik,[a] J.D. Jorgensen,[b] and S. Short[b]

[a] *Department of Physics, Northern Illinois University, FW 216, DeKalb, IL 60115, USA*
[b] *Materials Science Division, Argonne National Laboratory, Argonne, IL 60439, USA*

Received 18 April 2002; received in revised form 6 September 2002; accepted 25 September 2002

Abstract

Synthesis of new perovskite $Sr_{1-x-y}Ca_xBa_yMnO_{3-\delta}$ compounds is described in detail and dependence of their phase stability and structural distortions on the tolerance factor is discussed. Oxygen contents have been measured over extended temperature and composition ranges. Neutron powder diffraction was used to precisely measure the *A*–O and Mn–O bond lengths and derive accurate interatomic distances [Ca–O], [Sr–O], [Ba–O], and [Mn–O]. By using these parameters instead of tabulated ionic radii we have derived the functional dependence of the tolerance factor $t = t(x, y, T, \delta)$ on composition, temperature, and oxygen content. At a fixed oxygen content, the tolerance factor is an increasing function of temperature as a result of greater thermal expansion of the average $\langle A\text{–O}\rangle$ bond relative to the $\langle \text{Mn–O}\rangle$ bond. We find that the stability of the perovskite phase at high temperature is governed, as expected, by the magnitude of tolerance factor ($t \leqslant 1$) which can be adjusted by controlling the oxygen content $3-\delta$. This dependence of the tolerance factor on oxygen content and temperature can be utilized to design synthesis conditions for the controlled formation of the new, kinetically stable, perovskite phases.

Keywords: Tolerance factor; Manganites; Perovskites; Synthesis; Structural properties

1. Introduction

Perovskite manganites $AMnO_3$ have recently been studied in great detail because of very interesting magnetic and electronic properties resulting from competing charge, exchange, and phonon interactions. The properties can be tuned over a wide range through the choice of the size and valence of the cation on the *A*-site. The $La_{1-z}A_zMnO_3$ (A = Ca, Sr, Ba) systems have been studied most extensively [1,2]. These compounds show a strong correlation among interatomic distances and magnetic and structural transition temperatures [3]. Typical experimental studies of these materials are limited by the substitution level, z_s, of the *A* metal, beyond which formation of the perovskite phase is not possible because of the decreasing average size of the Mn^{3+z} ion and the unfavorable tolerance factor $t = [A\text{–O}]/2[\text{Mn–O}] \geqslant 1$ of the desired composition. Here, [*A*–O] and [Mn–O] are the average cation–oxygen interatomic distances of the *A*- and *B*-sites, respectively; the values of which can be obtained from the ionic sizes that are tabulated for various coordination numbers and oxidation states at room temperature [4]. One would expect to be able to synthesize the perovskite phase for atom sizes that give a tolerance factor as large as one. However, experimentally, tolerance-factor arguments have not been as successful as hoped for predicting the stability ranges of perovskite manganites. For example, it has been found experimentally [5] that the maximum substitution levels, z_s, when synthesis is done in air, are 1.0, 0.6, and 0.3 with increasing ionic size of A = Ca, Sr, and Ba ions, respectively. With modified synthesis methods at reduced oxygen pressure, z_s was recently extended for oxygen-deficient $La_{1-z}Sr_zMnO_{3-\delta}$ up to the end member of the phase diagram, $SrMnO_{3-\delta}$ ($z_s = 1$), and to ~ 0.5 for $La_{1-z}Ba_zMnO_{3-\delta}$ [6,7]. These results are in disagreement with the much smaller values of $z_s = 0.77$, 0.46, and 0.27, which are predicted for the Ca, Sr, and Ba compounds, respectively, based on tolerance-factor arguments using tabulated interatomic distances [4]. Additionally, since the tolerance factor usually increases with temperature, the discrepancy between calculated and observed z_s is larger still if the effect of a difference between the room and the synthesis temperatures is taken into account. Another example of

*Corresponding author. Fax: +815-753-8565.
E-mail address: dabrowski@anl.gov (B. Dabrowski).

0022-4596/03/$ - see front matter © 2002 Elsevier Science (USA). All rights reserved.
PII: S0022-4596(02)00056-7

the failure of tolerance-factor rules in perovskite compounds is associated with the ability to predict a transition from the distorted perovskite structure to a hexagonal structure when the A-site cation becomes very small. For $AMnO_3$ compounds (e.g., $YMnO_3$), this transition occurs at a tolerance factor less than or equal to about 0.85; while for other perovskite compounds such as YVO_3 and $YFeO_3$ the transition does not occur [8,9].

In this paper, we report the synthesis of $Sr_{1-x-y}Ca_xBa_yMnO_3$ compounds over an extended cation and oxygen composition range and establish the dependence of their phase stability and structural distortions on the tolerance factor. Neutron powder diffraction is used to precisely measure the A–O and Mn–O bond lengths and derive average $\langle A\text{–O}\rangle$ and $\langle \text{Mn–O}\rangle$ bond lengths, where weighted averages are defined to account for the unusual coordination of the A-site. Accurate interatomic distances [Ca–O], [Sr–O], [Ba–O], and [Mn–O], as well as tolerance factor are then obtained rather than relying on tabulated values. The temperature dependence of tolerance factor is obtained from measured average $\langle A\text{–O}\rangle$ and $\langle \text{Mn–O}\rangle$ bond lengths. Thermogravimetry is used to measure oxygen contents over extended temperature and composition ranges. By parameterizing measured tolerance factor, we obtain the functional dependence of the estimated tolerance factor $t_E = t(x, y, T, \delta)$ on composition, temperature, and oxygen content. At a fixed oxygen content, the tolerance factor is an increasing function of temperature as a result of greater thermal expansion of the average $\langle A\text{–O}\rangle$ bond relative to the $\langle \text{Mn–O}\rangle$ bond. We find that the stability of the perovskite phase at high temperature (where synthesis is done) is governed, as expected, by the magnitude of tolerance factor ($t \leqslant 1$), which can be adjusted by controlling the average size of the $Mn^{4-2\delta}$ ion as a function of the oxygen content $3-\delta$. This dependence of the tolerance factor on oxygen content and temperature can be utilized to design synthesis conditions for the controlled formation of the desired phases. Structural transitions of perovskite phase from cubic to tetragonal and then to orthorhombic appear at specific values of the tolerance factor that are the same for various compositions and temperatures. The results obtained in this way for manganites are potentially relevant for a wide range of perovskite materials with mixed-valent transition and post-transition metals.

The host compound for these studies is $SrMnO_3$. Under ambient conditions, $SrMnO_3$ forms a hexagonal four-layered structure with two layers consisting of face-sharing MnO_6 octahedra and two layers of corner-sharing octahedra as in the perovskite structure. The hexagonal MnO_6 network provides larger size cavities for Sr ions than the perovskite structure and, thus, is usually stable for large A-site ions such as Ba and Sr. Transformation of the oxygen-deficient four-layered hexagonal phase to the perovskite phase upon heating in air was studied by Negas and Roth [10]. These authors reported that the perovskite phase is stable above $\sim$1670 K (1400°C), where the oxygen content is reduced to 2.50–2.72. This low oxygen content stabilizes the perovskite phase because of the reduced valence, and resulting larger ionic size, of the Mn cation. Quenching from high temperatures where the perovskite phase is stable, followed by low-temperature annealing in air (at a temperature low enough that the cations do not diffuse), permitted Negas and Roth [10] to prepare a perovskite phase that was stoichiometric in oxygen content. Another similar method that stabilizes the perovskite phase [11,12] is reduction in argon flow at 1720 K (1450°C) resulting in an oxygen vacancy ordered $SrMnO_{2.5}$ compound that can also be easily re-oxidized at low temperatures.

We have recently studied the stability of the $SrMnO_{3-\delta}$ perovskite phase under a variety of oxygen partial pressures using "in situ" synthesis on a thermogravimetric apparatus [13]. In agreement with Negas and Roth [10], our results show that the perovskite phase forms at sufficiently high temperatures when the oxygen content is $\sim$2.5–2.71. Further reduction of the oxygen content below 2.5 results in decomposition of the perovskite phase. Full oxidation of the oxygen-deficient $SrMnO_{3-\delta}$ phase can be accomplished during annealing in air at temperatures as low as 470 K (200°C), while heating in air above 1020 K (750°C) results in transformation to the four-layered hexagonal phase. Such techniques, which allow the compositional phase diagram to be significantly expanded, were used to synthesize samples for the present study. Fig. 1 shows a schematic phase diagram for the $Sr_{1-x}Ca_xMnO_3$ system using these samples [14]. Upon decreasing the

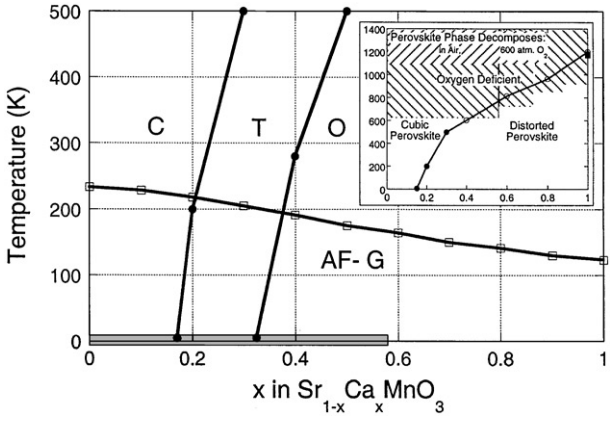

Fig. 1. Schematic phase diagram of structural and magnetic properties for $Sr_{1-x}Ca_xMnO_3$. The shadow bar denotes the extent of new compositions demanding a special synthesis procedure. Inset: Composition–temperature ranges of structural transitions, formation of oxygen vacancies, and stability of perovskite phase (legend the same as for main panel).

size of the *A*-site ion, a series of structural transitions appears at room temperature from cubic $Pm\bar{3}m$ to tetragonal *I4/mcm* (at $x \sim 0.3$) to orthorhombic *Pbnm* at $x \sim 0.4$. The magnetic structure remains G-type antiferromagnetic for all compositions, and T_N decreases from 233 to 125 K.

2. Sample preparation and experimental details

Polycrystalline $Sr_{1-x}Ca_xMnO_3$ ($0 \leqslant x \leqslant 1$) and $Sr_{1-y}Ba_yMnO_3$ ($y \leqslant 0.2$; Δx and Δy intervals of 0.1) samples were synthesized from stoichiometric mixtures of $CaCO_3$, $SrCO_3$, $BaCO_3$, and MnO_2. Samples were processed using the solid-state reaction method and fired in air several times at various temperatures up to 1620 K (1350°C) followed by slow cooling to 670 K (400°C). Using these conditions single-phase samples could be obtained only for $0.6 \leqslant x \leqslant 1$. The remaining compositions ($0 \leqslant x \leqslant 0.5$) and $y \leqslant 0.2$ were synthesized using a two-step method. In the first step, single-phase oxygen-deficient perovskites were obtained from precursors fired in flowing argon at temperatures increasing from 1420 K (1150°C) for $x = 0.5$ ($Sr_{0.5}Ca_{0.5}MnO_{2.68}$) to 1670 K (1400°C) for $x = 0$ ($SrMnO_{2.61}$). Synthesis of the Ba-substituted compositions $y = 0.1$ and 0.2 required careful control of the oxygen content near 2.5. This was accomplished by in situ synthesis of the samples on the Cahn TG171 thermobalance in 0.1% H_2/Ar forming gas at 1570 K (1300°C). However, even with this method we were unable to obtain single-phase perovskite samples with $y \geqslant 0.3$. In a second step, oxygen-deficient samples were annealed in air at 770 K (500°C) followed by slow cooling to bring the oxygen content to 3.00 ± 0.01 atoms per formula unit.

The effective oxygen contents were determined by TGA measurements with slow heating (1–2°C/min) and cooling (0.6°C/min) rates. Pure reaction gases of 100%, 20%, 1%, and 0.01% oxygen in argon (99.999%), H_2 (99.999%), and Ar (99.999%) as well as the gas mixtures of H_2/Ar were flowed at a rate of 100 cm^3 using an MKS gas flow controller. For increased accuracy about 2 g of small chunks were heated in Alumina crucibles suspended on Pt or Mo (for H_2/Ar reductions) wires. The weights of the samples were measured to a precision of 2 μg. Empty crucible TGA runs in pure gases and gas mixtures were used for calibration and buoyancy corrections. Reproducibility of the data was checked several times using identical TGA conditions for samples with the same *x*.

Time-of-flight neutron powder diffraction data were collected on the Special Environment Powder Diffractometer (SEPD) [15] at the Intense Pulsed Neutron Source (IPNS). Diffraction data were acquired at room temperature and for some selected samples at temperatures between 10 and 550 K using a closed-cycle helium refrigerator with heating capabilities. High-resolution backscattering data, from 0.5 to 4 Å, were analyzed using the Rietveld method with the General Structure Analysis System code (GSAS) [16].

3. Thermogravimetric measurements and synthesis

Data from a typical TGA measurement are shown in Fig. 2 for a perovskite sample of $Sr_{0.8}Ca_{0.2}MnO_{3-\delta}$ synthesized in Ar and annealed in air. The initial oxygen content 3.0, to which the TGA measurements were normalized, was determined by reduction of the material in 50% H_2/Ar to 1370 K (1100°C). During TGA measurement, the material was slowly heated to 1670 K (1400°C) and cooled to 670 K (400°C) in a 20% O_2/Ar gas mixture. Above ~620 K (350°C), the oxygen content begins to decrease during heating and reaches a value of 2.932 ± 0.002 at 1150 K (880°C)). On continued heating, there is a sudden increase of the oxygen content between 1150 K (880°C) and 1250 K (980°C) followed by a further decrease to 2.74 that is attained after a holding period of 1 h at 1670 K (1400°C). On cooling, the oxygen content gradually increases to 2.77 at 1600 K (1330°C) and then increases more rapidly to reach a final value of 3.00 below 1070 K (800°C).

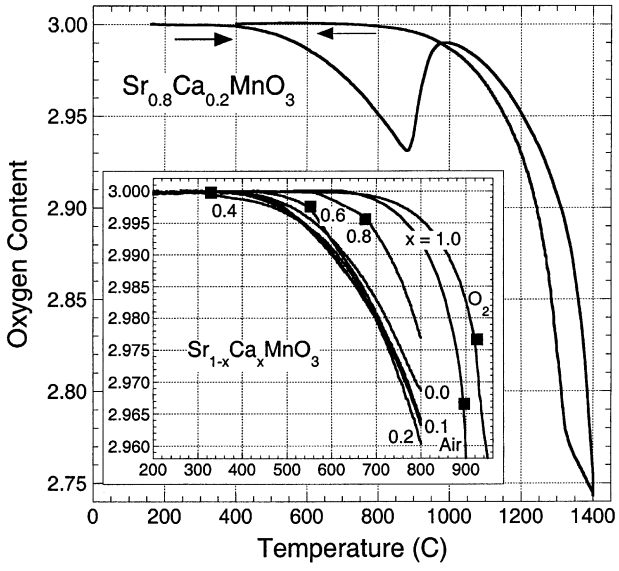

Fig. 2. Thermogravimetric analysis measurements on heating and cooling in a 20% O_2/Ar gas mixture for perovskite $Sr_{0.8}Ca_{0.2}MnO_3$. Inset: Oxygen nonstoichiometry during heating the perovskite phases $Sr_{1-x}Ca_xMnO_3$ ($x = 0.0$, 0.1, 0.2, 0.4, 0.6, 0.8, 1.0) in oxygen at low temperatures. Filled squares denote temperatures at which an increased formation of oxygen vacancies is observed on heating (legend the same as for main panel).

The observed changes of oxygen content are similar to changes that were observed for the $SrMnO_{3-\delta}$ sample [13] and, based on the X-ray diffraction measurements, can be interpreted as follows. When heated in air, the cubic perovskite $Sr_{0.8}Ca_{0.2}MnO_3$ compound begins to form oxygen vacancies around 620 K (350°C). The oxygen-deficient perovskite phase is kinetically stable to ~1150 K (880°C); above this temperature the perovskite phase is rapidly transformed to a hexagonal four-layered phase with significantly increased oxygen content (i.e., decreased amount of oxygen vacancies). Further heating introduces a larger amount of vacancies, and above ~1620 K (1350°C) a reverse transformation to the perovskite phase begins. The pure perovskite phase with a large amount of vacancies is achieved at 1670 K (1400°C). This phase is stable on cooling to 1600 K (1330°C) only when the oxygen content is in the range of 2.50–2.77, and then rapidly transforms to the hexagonal phase that is thermodynamically more stable for oxygen contents 2.77–3.00. The hexagonal phase displays a much higher stability against the formation of oxygen vacancies for temperatures 670–1150 K (400–880°C). This is consistent with the structural difference between the perovskite and the hexagonal phase for which oxygen atoms are bonded stronger to Sr and Mn cations within the layers of face-sharing MnO_6 octahedra.

Analogous phase transformations as a function of oxygen content and temperature were observed for $x = 0.0-0.5$. The range of stability of the perovskite phase as a function of oxygen content is enlarged for larger x. For $x = 0.6-1$, the range is so large that the perovskite phase remains stable in air for all temperatures. For these compositions, the amount of oxygen vacancies in air above ~1170 K (900°C) falls within the range of stability of the perovskite phase and thus the transformation to the hexagonal phase is not observed. By lowering the oxygen partial pressure during TGA experiments for $SrMnO_3$ [13], we have shown that temperature of the perovskite/hexagonal phase transition can be lowered by decreasing the oxygen content of the material, i.e., the perovskite phase can be obtained at lower temperatures. This information was used during synthesis of the $x = 0.0-0.5$ perovskite samples in Ar such that heating at excessively high temperatures in air was not required, thus avoiding the possible loss of Mn due to volatilization. The reverse effect, stabilization of the hexagonal phase, was observed during annealing at high-pressure oxygen. When the $x = 0.6-1$ perovskite samples (that are stable in air) were heated at 600 atm O_2 and 1270 K (1000°C), the $x = 0.6$ and 0.7 compositions transformed to hexagonal phase. Under high-pressure oxygen conditions the oxygen content of these compositions is increased and is apparently within the range of stability of the hexagonal phase.

The kinetics of decomposition of the perovskite phase was examined on a TGA in a 20% O_2/Ar gas mixture at 1070 K (800°C) for $x = 0.0-0.2$. The fraction of measured weight gain was associated with the fraction of the sample that transformed to hexagonal phase, and this relationship was subsequently confirmed by X-ray diffraction measurements. During a 12 h hold the $x = 0.0$ sample transformed completely to the hexagonal phase while only about 10% and 1% of the $x = 0.1$ and 0.2 samples changed to the hexagonal phase. Clearly, samples with increased Ca content require somewhat higher temperatures to achieve the phase transformation because the driving force for the phase transformation is decreasing due to increased stability range of the perovskite phase.

The inset of Fig. 2 shows oxygen nonstoichiometry during heating of perovskite phases in pure oxygen for several compositions at low temperatures. The oxygen content of the $x = 0.2$ sample in O_2 is slightly larger than in a 20% O_2/Ar gas mixture. All compositions $x = 0.0-0.6$ show virtually identical behavior to $x = 0.2$. Surprisingly, the highly Ca-substituted samples with $x = 0.8$ and 1 show much smaller amounts of oxygen vacancies. This behavior is contrary to the expected increased affinity towards formation of oxygen vacancies based on the lower electronegativity of Ca with respect to Sr. Apparently, there is another major effect that controls this behavior. Inspection of the TGA curves for $x = 0.4$, 0.6, 0.8, and 1.0 shows sudden changes of the slope at 600, 810, 960, and 1200 K (330°C, 540°C, 690°C, and 930°C), respectively, and at 1170 K (900°C) for the $x = 1.0$ sample in 20% O_2/Ar (denoted by the filled squares). For $x = 0.6$ and 0.8, the transition takes place for slightly nonstoichiometric samples while for $x = 1$ it arises for a larger oxygen vacancy concentration $\delta \sim 0.04$. Above these transition temperatures an accelerated formation of oxygen vacancies is observed. In the following sections, we will argue that on heating these temperatures may correspond to the transition from the distorted (orthorhombic or tetragonal) to the cubic perovskite structure. Using thermal analysis and high-temperature X-ray diffractometry in air, Taguchi et al. [17] detected orthorhombic/tetragonal and tetragonal/cubic structural transitions for $CaMnO_{3-\delta}$ at 1170 and 1186 K (896°C and 913°C), respectively. These temperatures agree very closely with our observed TGA transition at 1170 K (900°C) for the $x = 1.0$ sample in 20% O_2/Ar. This transition temperature is increased by 30 K in pure oxygen. The TGA results are summarized in the inset of Fig. 1 that displays composition–temperature ranges for structural transitions, formation of oxygen vacancies, and stability of the perovskite phase.

Similar tetragonal/cubic structural transitions appear below 570 K (300°C) for stoichiometric $x = 0.2$ and 0.3 samples while the $x = 0.0$ and 0.1 compositions remain

cubic to the lowest temperatures (see Fig. 1). For $x = 0.0-0.4$, the formation of oxygen vacancies begins already at low temperatures ~ 620 K (350°C) and occurs in the cubic structure. By comparing these structural transition temperatures with temperatures of accelerated formation of oxygen vacancies we can thus conclude that formation of oxygen vacancies is enhanced in the cubic structure when compared to the tetragonal or orthorhombic perovskite structures. Formation of oxygen vacancies is probably enhanced for $x < 0.8$ because of increasing crystal strain that is more important than the electronegativity difference between Sr and Ca. The TGA data and annealing experiments demonstrate that the crystallographic structure and stability of the perovskite phase are a function of the oxygen content, $3-\delta$, that controls the ionic size of the $Mn^{4-2\delta}$ ion which, in turn, affects the magnitude of the tolerance factor.

4. Determination of the room temperature bond lengths and tolerance factor

The two-step synthesis method allowed us to prepare for the first time $Sr_{1-x-y}Ca_xBa_yMnO_3$ compounds with the unusual tolerance factors $t \sim 1$ and investigate their structural and physical properties. Using precisely measured individual Mn–O and Sr(Ca, Ba)–O bond lengths, we have determined the average bond lengths $\langle$Mn–O$\rangle$ and $\langle A$–O$\rangle$ for several compositions with various crystal structures at room temperature. Average bond lengths were used to find accurate interatomic distances [Ca–O], [Sr–O], [Ba–O], and [Mn–O], and the tolerance factors, t, which are specific for perovskite manganites.

Fig. 3 shows measured individual A–O bond lengths for the 12-coordinated A-site and Mn–O bond lengths for the six-coordinated Mn at room temperature versus the calculated interatomic distance $[A\text{–O}]_S$. (The corresponding compositions can be read at the top of the figure.) For purposes of comparison, the interatomic distance $[A\text{–O}]_S$ was calculated here using values given by Shanon [4] for 12-coordinated Ca (1.34 Å), Sr (1.44 Å), and Ba (1.61 Å) and six-coordinated O (1.40 Å). Vertical lines on the graph separate structural ranges of orthorhombic, tetragonal, and cubic crystal structures. The individual A–O bonds have the same magnitudes for the cubic structure and differ among themselves only moderately for the tetragonal structure. There is considerable variance of the A–O bond lengths for the orthorhombic structure as a result of strongly distorted perovskite structure. We can observe that most of the measured A–O bond lengths are smaller than the calculated $[A\text{–O}]_S$ values indicating that ionic radii listed by Shanon overestimate the size of the A–O interatomic distances for Ca, Sr, and Ba for the perovskite

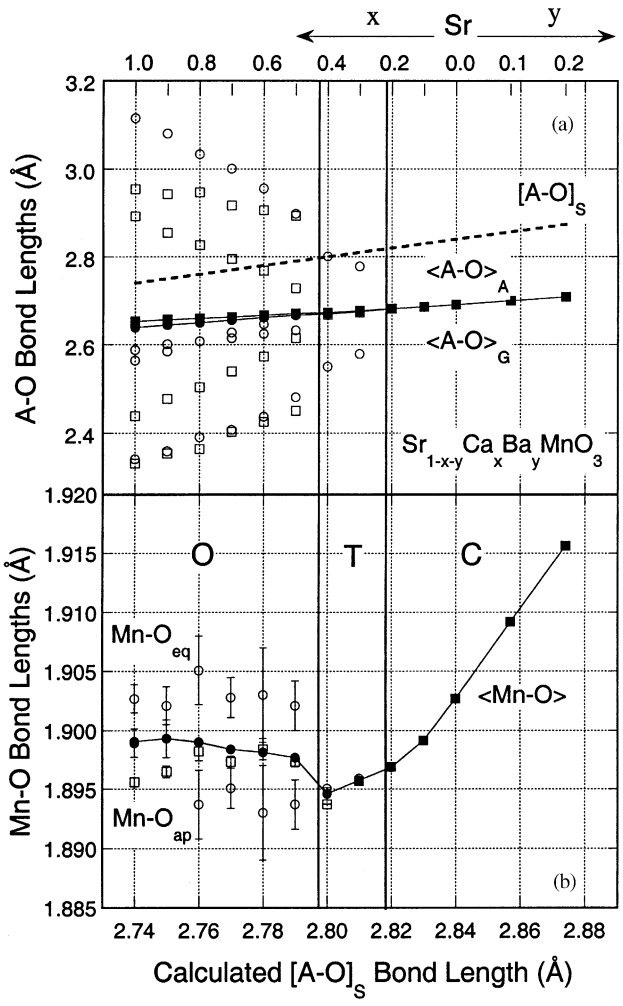

Fig. 3. Individual bond lengths measured at room temperature by neutron diffraction vs calculated interatomic distance $[A\text{–O}]_S$ (broken line on (a)) using values given by Shanon Ref. [4]. A–O bond lengths and their algebraic (filled squares, $\langle A\text{–O}\rangle_A$) and geometric (filled circles, $\langle A\text{–O}\rangle_G$) averages (see text) for 12-coordinated A-site (a) and equatorial and apical Mn–O bond lengths and their average $\langle$Mn–O$\rangle$ for six-coordinated Mn (b). Vertical lines on the graph separate structural ranges of orthorhombic (*Pbnm*), tetragonal (*I4/mcm*), and cubic ($Pm\bar{3}m$) crystal structures.

manganites. This indicates that a more accurate estimation of the interatomic distances specific for manganites should be possible from our experimental measured values for $Sr_{1-x-y}Ca_xBa_yMnO_3$ compounds than from the calculated effective radii that were derived from other materials.

The determination of the average bond length $\langle A$–O$\rangle$ is subject to some uncertainty for strongly distorted structures. The difficulty arises from the problem associated with assigning a unique A-site ionic coordination to oxygen when there is a considerable variance in the magnitude of individual bond lengths. Several authors have used nine-coordinated values of Ref. [4] for perovskites [2,3,18]. Using this coordination instead of the 12-coordinated ionic radii make them fictitiously

smaller and avoids the problem of the unusually long individual A–O bond lengths that would otherwise weigh too heavily during the algebraic averaging leading to artificially inflated values of the average bond length. In our case, we did not use this procedure as we wanted to apply the same unique averaging method over the whole range of substitutions that also includes the cubic and slightly distorted perovskite structures for which 12-coordination is clearly appropriate. Fig. 3(a) shows the results of two averaging methods, the common algebraic average $\langle A\text{–O}\rangle_A = (\Sigma_i\ (A\text{–O})_i)/12$ and the geometric average $\langle A\text{–O}\rangle_G = (\Pi_i\ (A\text{–O})_i)^{1/12}$ $(i = 1-12)$, both using a 12-coordinated environment for the A-site in $Sr_{1-x-y}Ca_xBa_yMnO_3$ compounds. The geometric averaging results in a smaller magnitude of the average bond for distorted structures as it puts less weight on longer bonds. Additionally, the dependence of $\langle A\text{–O}\rangle_G$ on Ca composition x (the calculated bond length $[A\text{–O}]_S$) is almost linear, while the algebraic average $\langle A\text{–O}\rangle_A$ shows characteristic upward curvature for highly distorted bonds. This increase of $\langle A\text{–O}\rangle_A$ for strongly distorted environment results from putting equal weight for short and strong bonds and for long and weak ones. It appears, thus, that the geometric averaging correctly includes effects of polyhedral distortion on the interatomic distances. As we will show in the following section, the geometric averaging leads to a better estimation of the interatomic distances [Ca–O], [Sr–O], and [Ba–O]. It should be pointed out that the other averaging procedures are also possible and it is not a goal of this paper to define the optimal averaging procedure. However, a reliable averaging procedure should lead to the same value of the average bond for various crystal distortions. This value is then used to define equilibrium interatomic distance while the effects of crystal distortions can be described separately as discussed by Shannon [4]. Another method of finding average bond lengths from bonding environments of different cations can use bond-valence sum analysis that have been applied successfully to mix-valent manganese perovskites [19].

The derived average bond lengths can be used to find interatomic distances from the relation $\langle A(x)\text{–O}\rangle = (1-x)[\text{Sr–O}] + (x)[\text{Ca–O}]$ and a similar equation for $\langle A(y)\text{–O}\rangle$. Estimation of the interatomic distance $[\text{Sr–O}] = 2.691 \pm 0.002$ Å was taken around $x = 0.1$ since both the algebraic and geometric averages have virtually the same value for cubic and tetragonal structures. Fig. 4(a) shows results of the calculation of interatomic distance [Ca–O] obtained by geometric and algebraic averaging. The geometric average gives the same magnitude of $[\text{Ca–O}] = 2.640 \pm 0.002$ Å for all x while algebraic average leads to compositionally dependent values that increase with distortion of the perovskite structure. It is worth noting that magnitudes of [Ca–O] obtained from geometrical and algebraic averaging

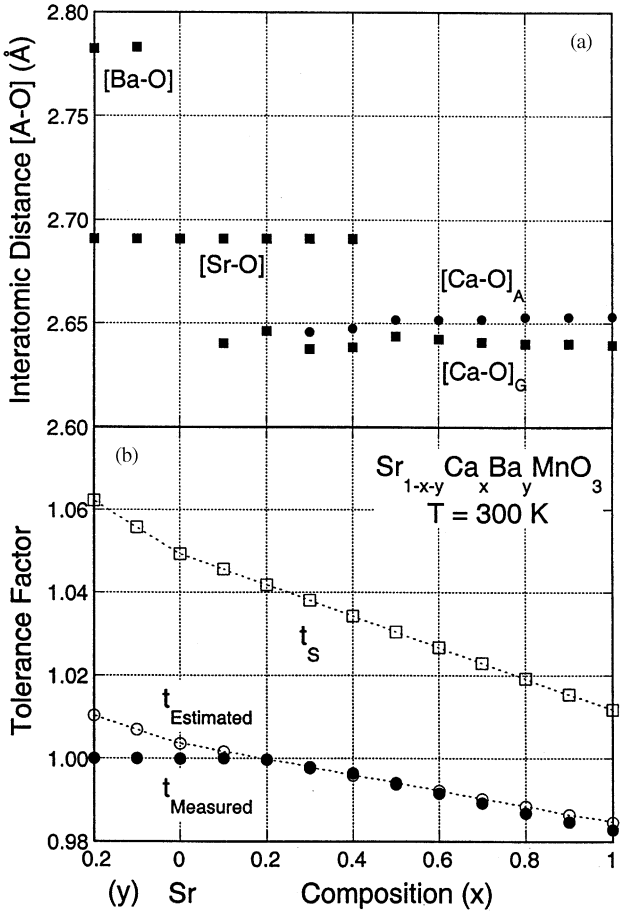

Fig. 4. (a) Calculated interatomic distances [Ba–O], [Sr–O], and [Ca–O] using geometric and algebraic averaging at room temperature for $Sr_{1-x-y}Ca_xBa_yMnO_3$. (b) Comparison of measured tolerance factors (filled circles) with estimated $t_E(x,y)$ (open circles, see text) and t_S (open squares) obtained by using interatomic distances $[A\text{–O}]_S$ and $[\text{Mn–O}]_S$ given by Shanon [4].

differ the most for pure $CaMnO_3$ $(x = 1)$ confirming the suitability of the geometric averaging procedure for the highly distorted structures. The derived interatomic distance $[\text{Ba–O}] = 2.783 \pm 0.004$ Å is less accurate because it was found based on only two data points $y = 0.1$ and 0.2 for lightly Ba-substituted samples. The interatomic distances derived here are significantly smaller than calculated from tables of Shannon [4].

The individual Mn–O bond lengths shown in Fig. 3(b) are the same for the cubic structure, virtually the same for the tetragonal structure, and differ among themselves only slightly for the orthorhombic structure. This is consistent with an almost undistorted octahedral coordination usually found for the $3d^3(t^3)$ Mn^{4+} ion. Measured Mn–O bonds are slightly larger than expected from Shanon's data (1.88 Å for six-coordinated Mn^{4+}). Because of almost identical individual Mn–O bond lengths, the average $\langle \text{Mn–O}\rangle$ does not depend on the averaging method and is ~ 1.898 and 1.895 Å for orthorhombic and tetragonal structures, respectively,

and increases significantly with the size of the A-site ion to ~ 1.915 Å for the cubic structure. The Mn–O bonds are relaxed to their equilibrium values for the tetragonal structure while they may be under slight tension for highly distorted orthorhombic structure. The Mn–O bonds are stretched beyond equilibrium values in the cubic structure to satisfy the dimensional constraints imposed by the symmetry and the sizes of the Sr and Ba ions. Based on these observations we have assigned the mean value found for tetragonal and orthorhombic structures 1.896 ± 0.02 Å as a characteristic [Mn–O] interatomic distance at room temperature.

Using the reliable interatomic distances [Ca–O], [Sr–O], [Ba–O], and [Mn–O], the estimated tolerance factor of the perovskite phase is defined as $t_E(x,y) = ((1-x-y)[\mathrm{Sr-O}]+x[\mathrm{Ca-O}]+y[\mathrm{Ba-O}])/2[\mathrm{Mn-O}]$ and can be calculated for any combination of Ca, Sr, and Ba atoms on the A-site. Fig. 4(b) shows a comparison of several tolerance factors as a function of composition at 300 K. The estimated t_E represents very well the measured tolerance factors for $t \leqslant 1$, while the tolerance factor t_S (obtained by using interatomic distances $[A\text{–O}]_S$ and $[\mathrm{Mn–O}]_S$ given by Shanon [4]) substantially overestimates these values. The difference between measured tolerance factor t and t_E for $t_E > 1$ is a measure of the tension imposed on the Mn–O bond in the cubic structure; clearly, the experimentally determined t can not be larger than 1. The defining of reliable interatomic distances [Ca–O], [Sr–O], [Ba–O], and [Mn–O] which enables the calculation of the estimated tolerance factor t_E is of great value for crystallographers and physicists since, as was shown for manganites, these quantities control to a large extent the structural and physical properties near room temperature. They can be used to predict, for example, the magnetic and resistive behavior and the magnetic transition temperatures for various compositions [14].

5. Temperature dependence of the tolerance factor and relationship to structural distortions

Knowledge of the tolerance factor for various compositions at high temperatures, 1070–1670 K (800–1400°C), is important for synthetic chemists as it enables prediction of feasible substitutions and solubility limits without resorting to actual preparation of these materials. Since interatomic bond lengths expand with increasing temperature, it is expected that the tolerance factor is also a function of temperature. In addition as it was shown from TGA measurements for $T > \sim 730$ K (350°C), the oxygen content is not constant, i.e., the valence state of Mn is changing, and so is its bond length to oxygen. In this section, we estimate the temperature dependence of the tolerance factor for stoichiometric compositions. This estimate should be valid for $T < 800$ K when $x = 0-0.6$, $T < 900$ when $x \sim 0.8$, and $T < 1050$ K for $x = 1$ because oxygen deficiency remains quite small ($\delta < 0.005$) below these temperatures. The effect of larger oxygen nonstoichiometry will be discussed in the next section.

Using precisely measured Mn–O and Sr(Ca, Ba)–O bond lengths for several compositions as a function of temperature, we have determined the temperature dependence of the average bond lengths $\langle \mathrm{Mn–O} \rangle$ and $\langle A\text{–O} \rangle_G$, the tolerance factor $t(x,y,T)$, and their relation to distortions of perovskite manganites. Fig. 5(a)–(c) shows the measured average bond lengths $\langle A\text{–O} \rangle_G$ and $\langle \mathrm{Mn–O} \rangle$, and tolerance factor $t(x,y,T) = \langle A\text{–O} \rangle_G / 2\langle \mathrm{Mn–O} \rangle$ as a function of temperature for $x = 0.3$, 0.4, 0.5, and 0.9. We can observe that, in general, both bond lengths increase with temperature, the $\langle A\text{–O} \rangle_G$ bond showing much faster

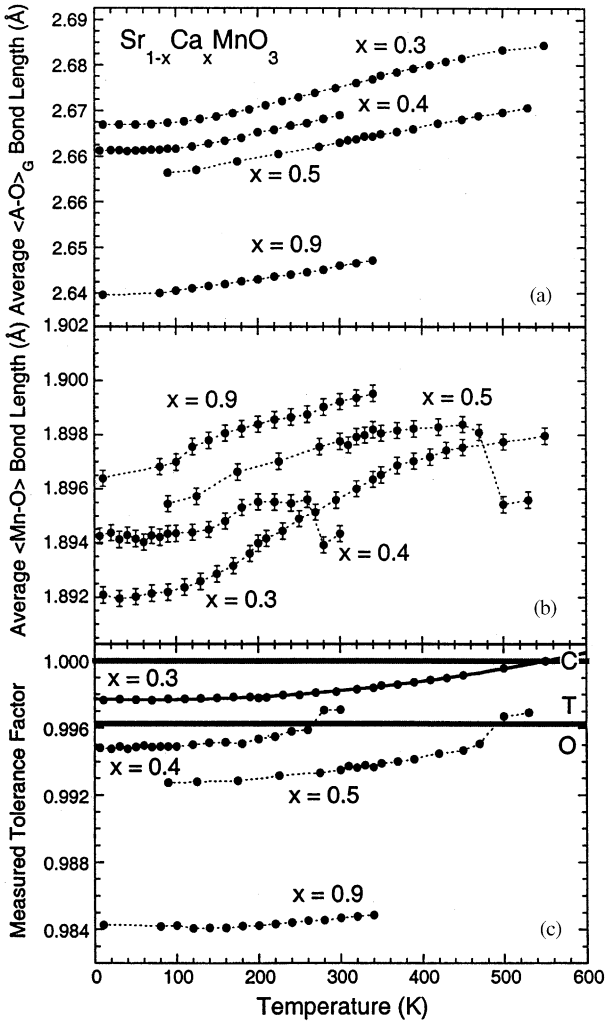

Fig. 5. Average bond lengths $\langle A\text{–O} \rangle_G$ (a), $\langle \mathrm{Mn–O} \rangle$ (b), and tolerance factor $t(x,y,T) = \langle A\text{–O} \rangle_G / \langle \mathrm{Mn–O} \rangle$ as a function of temperature for $x = 0.3$, 0.4, 0.5, and 0.9. Horizontal lines at $t = 1.0$ and 0.996 on (c) denote divisions between stability ranges of cubic (C), tetragonal (T), and orthorhombic structure (O).

and smoother variation. There is a slight decrease of the $\langle$Mn–O$\rangle$ bond on heating at the orthorhombic/tetragonal transition that coincides with a change of the tilt pattern of the rotated $Mn–O_6$ octahedra [14]. The tolerance factor (Fig. 5(c)) is almost constant below ~ 200 K and above this temperature increases at a faster rate. There is a slight additional increase of tolerance factor near 0.996 at the orthorhombic/tetragonal transition for both $x = 0.4$ and 0.5 at 480 and 270 K, respectively, indicating that it is primarily the magnitude of the tolerance factor that controls the orthorhombic/tetragonal structural transition for various compositions and temperatures. Approach of the tolerance factor to 1.0 denotes the transition to cubic structure for $x = 0.3$ at ~ 500 K.

We have estimated the temperature dependence of the measured tolerance factor by using a least squares fit to the quadratic formula $t_E(x,y,T) = t_0 + t_1 T + t_2 T^2$. The parameter $t_0 = t_0(x,y) = 1.0030 - 0.0190x + 0.0343y$ is the tolerance factor at 0 K for various x and y compositions. The other derived parameters, $t_1 = t_1(x) = (-0.836 - 2.399x)10^{-6}\,K^{-1}$, and $t_2 = t_2(x) = (0.978 + 0.541x)10^{-8}\,K^{-2}$ were also found to depend on composition, x. These parameters give an excellent fit over 0–550 K for compositions $x = 0.3$ and 0.5. For $x = 0.4$ and 0.9, fits are less reliable and achievable only over a narrower temperature range 0–350 K. The solid curve in Fig. 5(c) shows a fit for $x = 0.3$. Unfortunately, we could not use for fitting purposes the high quality data acquired for compositions $y = 0.1$ and $x = 0.0$ and 0.1 because for these compositions the structure remains cubic over the whole temperature range and the measured $t(T) = 1$. For this reason, we could not obtain the dependence of t_1 and t_2 on Ba content, y, and we were constrained to use the same constant parameters $t_1(x = 0)$ and $t_2(x = 0)$ for all y.

Fig. 6 summarizes the derived results by showing the estimated tolerance factor $t_E(x,y,T) = t_0(x,y) + t_1(x)T + t_2(x)T^2$ for $Sr_{1-x-y}Ca_xBa_yMnO_3$ compounds at several temperatures between 0 and 1500 K as a function of the calculated interatomic distance [A–O] = (1−x−y)[Sr–O] + (x)[Ca–O] + (y)[Ba–O]. The horizontal lines at $t = 1.0$ and 0.996 denote divisions between the stability ranges of cubic, tetragonal, and orthorhombic structures. The graph can be read to predict structural ranges as a function of temperature and composition while using only the derived quantities. It correctly describes the observed structural transitions for $x = 0.3$ (cubic/tetragonal), 0.4 (tetragonal/orthorhombic), and 0.5 (tetragonal/orthorhombic) at ~ 500, 350, and 500 K, respectively, and estimates the tetragonal/orthorhombic transition for $CaMnO_3$ at $T > 1100$ K.

We should stress that the parameters of the quadratic formula were derived here for oxygen stoichiometric compositions, 3.0, i.e., the fit is valid for manganites

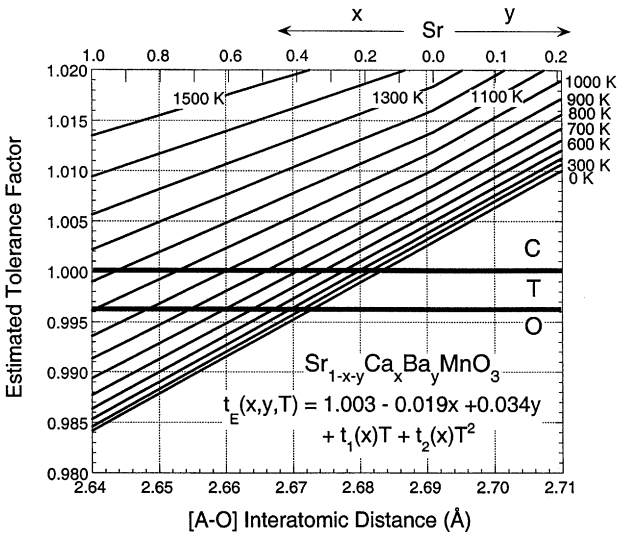

Fig. 6. Estimated tolerance factor $t_E(x,y,T)$ (see text) for temperatures 0–1500 K as a function of calculated interatomic distance [A–O] = (1−x−y)[Sr–O] + (x)[Ca–O] + (y)[Ba–O]. The horizontal lines at $t = 1.0$ and 0.996 divide stability ranges of cubic, tetragonal, and orthorhombic structures.

only over a limited range at elevated temperatures. For example, the experimentally observed orthorhombic/tetragonal and tetragonal/cubic transitions for $CaMnO_3$ occur in air at higher temperatures, 1169 and 1186 K (896°C and 913°C) [17], than predicted for stoichiometric compounds, ~ 1000 and 1130 K, respectively, due to the presence of oxygen vacancies. However, similar fits should be valid over extended temperature range for several fixed oxidation state ions; for example, Sc, Ti, Zr, Sn, and Al and several other ions for which oxygen vacancies do not appear in large amounts in perovskites; for example, Ru, Ir, and Mo.

6. Dependence of the tolerance factor on oxygen content and relationship to phase stability

Our TGA measurements have shown that the formal valence state of $Mn^{4-2\delta}$ is decreasing for $T > 620$ K (350°C) due to formation of oxygen vacancies δ. The Mn–O bond length is known to increase as a function of decreasing oxidation state of Mn; for example, using Shanon's data [4] the interatomic distance $[Mn^{3+}–O]_S = 1.995$ Å for a six-coordinated ion is considerably larger than for an Mn^{4+} (1.88 Å). Evaluation of the interatomic distance $[Mn^{4-2\delta}–O] = (1–2\delta)[Mn^{4+}–O] + (2d)[Mn^{3+}–O]$ is complicated by the fact that the magnitude of the interatomic distance $[Mn^{3+}–O]$ is uncertain due to the Jahn-Teller distorted environment of the d^4 Mn^{3+} ion at room temperature. The measured Mn^{3+}–O bond lengths vary in size from 1.901 to 2.189 Å while their algebraic average was reported over a range of 2.012–2.017 Å [20].

Fortunately, we can use more reliable high temperature values to determine the magnitude of [Mn^{3+}–O] since the Jahn-Teller distortion decreases with increasing temperature and disappears above ~ 750 K (480°C) for $LaMnO_3$ [20]. It is thus useful to use the [Mn^{3+}–O] = 2.011 Å value measured for the more symmetrical environment of the d^4 Mn^{3+} ion with individual bonds lengths in the range 1.988–2.035 Å at 798 K. [20] Based on our data, the estimated value of [Mn^{4+}–O] = 1.906 Å at this temperature. Using these values and separating the dependence of the tolerance factor on oxygen deficiency δ (or the valence of $Mn^{4-2\delta}$) we get the final formula $t_E(x,y,T,\delta) = t_E(x,y,T)\{1-0.055(2\delta)\}$, where $t_E(x,y,T)$ was given in the previous section for oxygen stoichiometric compositions.

Fig. 7 shows the estimated tolerance factor $t_E(x,y,T=1600\,K,\ \delta)$ for several oxygen vacancy contents between 0 and 0.5 as a function of calculated interatomic distance [*A*–O] at a typical synthesis temperature 1600 K (1330°C). The presence of oxygen vacancies dramatically reduces the magnitude of the tolerance factor. With increasing δ, the region of compositions with $t_E \leqslant 1$ is gradually enlarged reaching $x = 0.2$, 0.0, and $y = 0.2$ for $\delta \approx 0.23$, 0.25, and 0.31, respectively. The magnitudes of oxygen deficiency found for $x = 0.2$ and 0.0 are very similar to the values corresponding to the perovskite-to-hexagonal phase transition observed from TGA and X-ray measurements [10,13]. This correlation indicates that the stability of the perovskite phase at synthesis temperature is limited by the condition $t_E(x,y,T,\delta) \leqslant 1$. The graph can be used to predict the phase stability as a function of composition, temperature, and oxygen content and to design optimum synthesis conditions to produce the desired phases.

By determining the oxygen vacancy content, δ, with TGA measurements and using the derived dependence of the estimated tolerance factor $t_E(x,y,T,\delta)$, we can calculate its value as a function of temperature. Fig. 8 shows an example of such a calculation for $Sr_{0.8}Ca_{0.2}MnO_3$ using the TGA data presented in Fig. 2. The tolerance factor of the stoichiometric, cubic perovskite phase at the beginning of the TGA experiment is just slightly larger than 1.0. (On cooling, the sample transforms to tetragonal structure at ~ 200 K with $t < 1.0$; see Fig. 1.) The tolerance factor increases on heating, putting Mn–O bonds under increased tension. Above ~ 620 K (350°C), oxygen vacancies begin to form leading to a slower increase of the tolerance factor than expected for stoichiometric material as depicted by the $t_E(T,\delta=0)$ curve. On continued heating, the tolerance factor starts to decrease with increasing δ, however, it still remains considerably larger than 1.0 up to 1150 K (880°C). In the temperature range 1150–1250 K (880–980°C) there is a rapid increase of the tolerance factor caused by a sudden increase of the oxygen content during the transition to the hexagonal phase. Further heating induces a rapid decrease of the tolerance factor below 1.0 caused by a sharp decrease of the oxygen content and transformation to the perovskite phase at 1670 K (1400°C). On cooling, the tolerance factor gradually increases when $t_E(T,\delta) \leqslant 1.0$ at 1600 K (1330°C) and then increases more rapidly when $t_E(T,\delta) > 1.0$ during the reversed transition to hexagonal phase. The dependence of the observed phases on

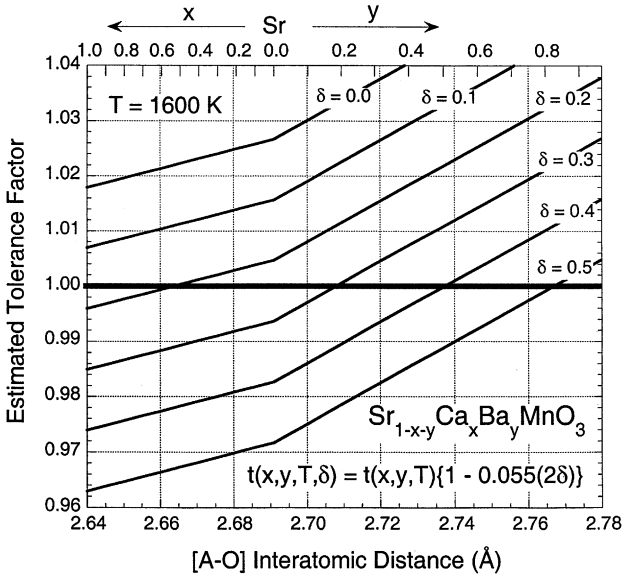

Fig. 7. Estimated tolerance factor $t_E(x,y,T,\delta)$ for oxygen vacancy concentrations $\delta = 0$, 0.1, 0.2, 0.3, 0.4, and 0.5 at 1600 K (1330°C) as a function of calculated interatomic distance [*A*–O].

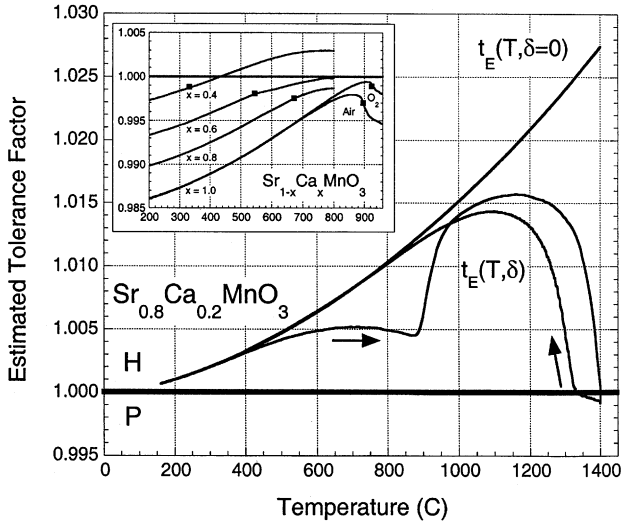

Fig. 8. Estimated tolerance factor $t_E(x,y,T,\delta)$ as a function of temperature calculated using oxygen vacancy concentration δ from TGA data shown in Fig. 2 for $Sr_{0.8}Ca_{0.2}MnO_3$. Inset shows expected tolerance factor calculated for $x = 0.4$, 0.6, 0.8, and 1.0 samples using TGA data presented in inset to Fig. 2 (Legend the same as for main panel).

the magnitude of the tolerance factor confirms that the stability of the perovskite phase is limited by the condition $t_E(x,y,T,\delta) \leqslant 1.0$ at synthesis temperatures $T > \sim 1070$ K (800°C). Despite this condition, it is still possible to obtain kinetically stable perovskite phases with $t > 1.0$ at lower temperatures $T < \sim 1070$ K (800°C) by a two-step procedure that produces an oxygen-deficient perovskite phase with $t < 1.0$ at elevated temperature followed by a low-temperature oxygen anneal that makes $t > 1.0$. Knowledge of the functional dependence of the tolerance factor on composition, temperature, and oxygen vacancy concentration allows preparation of a wide range of new perovskite manganites and other mixed-valent compounds by the two-step procedure. For example, using this method we were recently able to extend the solubility limit, z_s, to 0.7 for $La_{1-z}Ba_zMnO_3$ [21].

The inset of Fig. 8 shows the estimated tolerance factor calculated for $x = 0.4$, 0.6, 0.8, and 1.0 samples using TGA data presented in the inset of Fig. 2. With increasing temperature, the tolerance factor increases towards 1.0, however, for $x = 1.0$, 0.8, and 0.6, it remains below 1.0 due to a sufficient amount of induced oxygen vacancies. For $x = 0.4$ and all $x = 0.0-0.5$ (not shown), there are not enough oxygen vacancies formed, so t becomes larger than 1.0. These are exactly the compositions that exhibit a transition to the hexagonal phase in agreement with previous observations that the perovskite is unstable when $t > 1$ above 800 K. It is interesting to observe that the tolerance factor would exceed 1.0 also for compositions $x = 0.6-1.0$ if not for an accelerated formation of oxygen vacancies when t approaches 1.0 at temperatures denoted by filled squares. It appears that for these compositions the system prefers to remain in the perovskite phase with larger amounts of oxygen vacancies rather than decomposing to the hexagonal phase. Since, for this range of temperatures the perovskite phase assumes cubic symmetry, it is possible that the developing tension exerted on the Mn–O bonds is relieved more easily by accelerated formation of oxygen vacancies rather than by a broad rearrangement of the A–O and Mn–O coordinations in the hexagonal structure.

7. Conclusion

By directly measuring the dependence of individual Mn–O, Sr–O, Ca–O, and Ba–O bond lengths on composition for perovskite manganites we have determined room temperature interatomic distances [Ca–O] = 2.640 ± 0.002, [Sr–O] = 2.691 ± 0.002, [Ba–O] = 2.783 ± 0.004, and [Mn^{4+}–O] = 1.896 ± 0.02 Å suitable for estimating the magnitude of the tolerance factor $t_E(x,y) = ((1-x-y)[\text{Sr–O}] + x[\text{Ca–O}] + y[\text{Ba–O}])/2[\text{Mn–O}]$ for $Sr_{1-x-y}Ca_xBa_yMnO_3$ compounds. This quantity is very useful for predicting the structural and physical properties near room temperature. Using the temperature dependence of the bond lengths, we have parameterized the tolerance factor as a function of temperature for stoichiometric compositions to yield $t_E(x,y,T) = t_0 + t_1T + t_2T^2$ where $t_0 = 1.0030 - 0.0190x + 0.0343y$ is a tolerance factor at 0 K, $t_1 = (-0.836-2.399x)10^{-6}$ Å/K, and $t_2 = (0.978 + 0.541x)10^{-8}$ Å/K^2. Finally, by estimating the dependence of the interatomic distance [$Mn^{4-2\delta}$–O] on oxygen vacancy concentration, δ, we have derived an estimated tolerance factor as a function of composition, temperature, and oxygen vacancy concentration $t_E(x,y,T,\delta) = t_E(x,y,T)\{1-0.055(2\delta)\}$. Knowledge of $t_E(x,y,T,\delta)$ at high temperatures 1070–1670 K (800–1400°C) is important for predicting feasible substitutions and solubility limits and designing optimum synthesis conditions to produce the desired phases. The parameterization method of $t_E(x,y,T,\delta)$ developed for manganites can be extended to more complex $R_{1-z}A_zMn_{1-w}B_wO_3$ (R = Rare Earth's; A = Ca, Sr, Ba; B = transition and post-transition metals, $z = 0-1$, $w = 0-1$) systems enabling production of a vast range of novel compounds through appropriately designed synthesis methods.

We have recently investigated [14] $Sr_{1-x-y}Ca_xBa_yMnO_3$ perovskites in order to determine the size effect of the A-site on the antiferromagnetic transition temperature T_N. The observed variation of T_N (Fig. 1) was satisfactorily described as a function of $\langle \cos^2\theta \rangle$ of the Mn–O–Mn bond angle related to the superexchange interaction integral, and σ^2, the A-site ionic size variance [14]. Since the Mn–O–Mn bond angle can be also expressed as a function of the A–O and Mn–O bond lengths, the equivalent description of T_N can be achieved in terms of tolerance factor $t(x,y)$ and σ^2. The previously available tabulated interatomic distances were not accurate enough to be used for this purpose as is evident from the discrepancy between calculated and observed interatomic distances. Our more accurate interatomic distances derived here for manganites should be used for this purpose. Unusually short lattice parameter ($a_0 = 3.805$) (and interatomic distance of [Sr–O] = $a_0/\sqrt{2} \sim 2.69$ Å) for manganites when compared with the lattice parameters $a_0 = 3.869$, 3.841, and 3.904 for several cubic perovskites $SrBO_3$ with B = Fe, V, and Ti, respectively, may be a cause of the discrepancies. The [A–O] interatomic distances derived here for $Sr_{1-x-y}Ca_xBa_yMnO_3$ manganites correctly describe also the tolerance factor, solubility limits, and structural distortions for the $La_{1-x}Sr_xMnO_3$ and $Pr_{1-x}Sr_xMnO_3$ perovskite systems over a wide range of substitutions with $x > 0.2$ [5]. For $0.2 \geqslant x \geqslant 0.0$ noticeable discrepancies are observed caused by appearance of the coherent Jahn-Teller distortions. It remains to be investigated if these discrepancies can be removed by the

derivation of two different equilibrium interatomic distances for Mn^{3+} corresponding to localized and itinerant cases. Future work should also check if our interatomic distances would correctly describe other manganite structures and how well the developed method of parameterized tolerance factor as a function of composition, temperature, and oxygen content would describe other transition metal perovskites.

Acknowledgments

Work at NIU was supported by the ARPA/ONR, NSF-DMR-0105398, and by the State of Illinois under HECA. At ANL work was supported by the US Department of Energy, Office of Science under Contract No. W-31-109-ENG-38.

References

[1] A. Urushibara, Y. Moritomo, T. Arima, A. Asamitsu, G. Kido, Y. Tokura, Phys. Rev. B 51 (1995) 14103.
[2] P. Schiffer, A.P. Ramirez, W. Bao, S.-W. Cheong, Phys. Rev. Lett. 75 (1995) 3336.
[3] H.Y. Hwang, S.-W. Cheong, P.G. Radaelli, M. Marezio, B. Batlogg, Phys. Rev. Lett. 75 (1995) 914–917.
[4] R.D. Shannon, Acta Crystallogr. A 32 (1976) 751.
[5] B. Dabrowski, K. Rogacki, X. Xiong, P.W. Klamut, R. Dybzinski, J. Shaffer, J.D. Jorgensen, Phys. Rev. B 58 (1998) 2716;
O. Chmaissem, B. Dabrowski, J. Mias, S. Kolesnik, J.D. Jorgensen, S. Short, unpublished.
[6] K. Kikuchi, H. Chiba, M. Kikuchi, Y. Syono, J. Solid State Chem. 146 (1999) 1.
[7] F. Millange, V. Caignaert, B. Domenges, B. Raveau, E. Suard, Chem. Mater. 10 (1998) 1974.
[8] H.L. Yakel, W. Koehler, E.F. Bertaut, E.F. Forrat, Acta Crystallogr. 16 (1963) 957.
[9] B.B. van Aken, A. Meetsma, T.T.M. Palstra, Acta Crystallogr. C 57 (2001) 230.
[10] T. Negas, R.S. Roth, J. Solid State Chem. 1 (1970) 409.
[11] V. Caignaert, J. Magn. Magn. Mater. 166 (1997) 117.
[12] K.R. Poeppelmeier, M.E. Loenowicz, J.C. Scanion, J.M. Longo, W.B. Yelon, J. Solid State Chem. 45 (1982) 71.
[13] J. Mais, B. Dabrowski, O. Chmaissem, S. Kolesnik, unpublished.
[14] O. Chmaissem, B. Dabrowski, S. Kolesnik, J. Mais, D.E. Brown, R. Kruk, P. Prior, B. Pyles, J.D. Jorgensen, Phys. Rev. B 64 (2001) 134412.
[15] J.D. Jorgensen, J.J. Faber, J.M. Carpenter, R.K. Crawford, J.R. Haumann, R.L. Hitterman, R. Kleb, G.E. Ostrowski, F.J. Rotella, T.G. Worton, J. Appl. Crystallogr. 22 (1989) 321.
[16] A.C. Larson, R.B. von Dreele, General Structure Analysis System, University of California, 1985–1990.
[17] H. Taguchi, M. Nagao, T. Sato, M. Shimada, J. Solid State Chem. 78 (1989) 312.
[18] L.M. Rodriguez-Martinez, J.P. Attfield, Phys. Rev. B 54 (1996) R15622.
[19] G.H. Rao, K. Barner, I.D. Brown, J. Phys.: Condens. Matter 10 (1998) L757.
[20] J. Rodriguez-Carvajal, M. Hennion, F. Moussa, A.H. Moudden, L. Pinsard, A. Revcolevschi, Phys. Rev. B 57 (1998) R3189.
[21] B. Dabrowski, O. Chmaissem, J. Mias, S. Kolesnik, J.D. Jorgensen, unpublished.